

Role of Oxygen Holes in Li_xCoO_2 Revealed by Soft X-Ray Spectroscopy

T. Mizokawa, Y. Wakisaka, and T. Sudayama

Department of Physics and Department of Complexity Science and Engineering, University of Tokyo, Chiba 277-8561, Japan

C. Iwai, K. Miyoshi, and J. Takeuchi

Department of Material Science, Shimane University, Matsue 690-8504, Japan

H. Wadati

Department of Applied Physics and Quantum-Phase Electronics Center, University of Tokyo, Hongo, Tokyo 113-8656, Japan

D. G. Hawthorn

Department of Physics and Astronomy, University of Waterloo, Waterloo, Ontario N2L 3G1, Canada

T. Z. Regier

Canadian Light Source, University of Saskatchewan, Saskatoon, Saskatchewan S7N 0X4, Canada

G. A. Sawatzky

Department of Physics and Astronomy, University of British Columbia, Vancouver, British Columbia V6T 1Z1, Canada

(Received 22 March 2013; published 2 August 2013)

The fundamental electronic structure of the widely used battery material Li_xCoO_2 still remains a mystery. Soft x-ray absorption spectroscopy of Li_xCoO_2 reveals that holes with strong O $2p$ character play an essential role in the electronic conductivity of the $\text{Co}^{3+}/\text{Co}^{4+}$ mixed valence CoO_2 layer. The oxygen holes are bound to the Co^{4+} sites and the Li-ion vacancy, suggesting that the Li-ion flow can be stabilized by oxygen hole back flow. Such an oxygen hole state of Li_xCoO_2 is unique among the various oxide-based battery materials and is one of the key ingredients to improving their electronic and Li-ion conductivities.

DOI: [10.1103/PhysRevLett.111.056404](https://doi.org/10.1103/PhysRevLett.111.056404)

PACS numbers: 71.28.+d, 78.70.Dm, 75.25.Dk

Although Li_xCoO_2 is widely used as the cathode material of Li-ion batteries, it is not well understood how the high Li-ion mobility is related to the electronic structure of the CoO_2 triangular lattice layer of Li_xCoO_2 . In the ground breaking paper by the Goodenough group [1], it has been pointed out that late transition-metal oxides with high valence states can sustain high cell voltages and high current densities due to their good electronic conduction. In general, mixed valence transition-metal oxides with higher valence tend to be conductive. This tendency can be understood on the basis of the Zaanen-Sawatzky-Allen scheme [2] in which the charge-transfer energy from the O $2p$ level to the transition-metal $3d$ level decreases with the transition-metal valence [3]. In Li_xCoO_2 with Co^{3+} and Co^{4+} , it is expected that the O $2p$ level is almost degenerate with the Co $3d$ level, and both the Co $3d$ and O $2p$ states can contribute to the electronic conduction. In addition, the importance of the O $2p$ level has been revealed in the *ab initio* theory on Li_xCoO_2 by Aydinol *et al.* who established that the substantial charge transfer to the oxygen site is responsible for the large voltage difference of Li_xCoO_2 [4]. Therefore, a deeper understanding of the complicated electronic structure including Co $3d$ and O $2p$ states in Li_xCoO_2 is very useful for finding a strategy to enhance the Li-ion mobility of more stable cathode materials such as Li_xFePO_4 [5], resulting in improving battery performance.

Layered cobalt oxides, which have CoO_2 triangular lattices with $\text{Co}^{3+}/\text{Co}^{4+}$ mixed valence, exhibit a rich variety of physical properties, such as superconductivity [6], large thermoelectric power [7], and various phase transitions [8]. Among them, Li_xCoO_2 , which consists of CoO_2 layers and interlayers of Li atoms alternatively stacked along the c axis, has been intensively investigated as a cathode material for Li-ion batteries [1,9–11] and a useful thermoelectric material [12–14]. In Li_xCoO_2 , the CoO_2 triangular lattice layer consists of edge-sharing CoO_6 octahedra as shown in Fig. 1(a). The five Co $3d$ orbitals are split into two e_g orbitals and three t_{2g} orbitals under the cubic ligand field, and the three t_{2g} orbitals are further split into one a_{1g} orbital and two e'_g orbitals under the trigonal ligand field. The ligand field splitting is mainly due to the anisotropic hybridization between the Co $3d$ orbitals and the O $2p$ orbitals, and, therefore, the O $2p$ components are mixed into the Co $3d$ states. Figure 1(b) shows the electronic configurations of the Co^{3+} and Co^{4+} ions. The Co^{3+} ions are in a low-spin state (t_{2g}^6) with $S = 0$ and the Co^{4+} ions are in a low-spin state (t_{2g}^5) with $S = 1/2$ [15,16]. Since the O 1s XAS is due to electronic transitions from the O 1s core level to the unoccupied Co $3d$ levels with the O $2p$ components, it is very sensitive to the local electronic configuration of the Co ions. When an O 1s core electron is excited at the oxygen

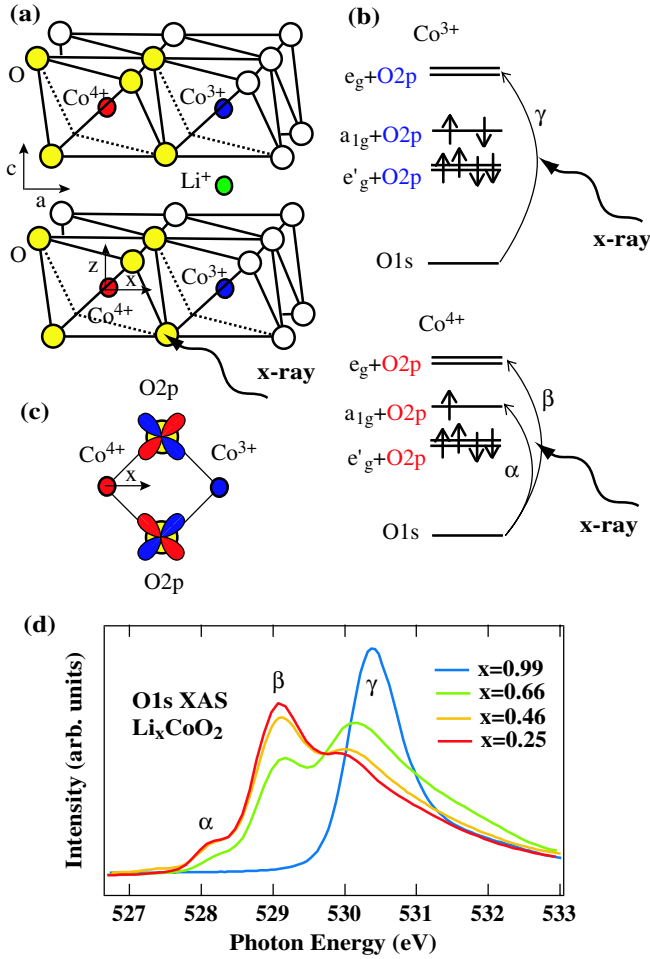


FIG. 1 (color online). O 1s x-ray absorption spectroscopy. (a) Schematic crystal structure of Li_xCoO_2 . Co ions are surrounded by six oxygen ions and form a triangular lattice layer. Li ions are sandwiched by the Co-O layers. The oxygen sites with higher O 2p hole concentration are indicated by the yellow (shaded) circles. (b) Electronic configurations and O 1s XAS processes for the Co^{3+} and Co^{4+} sites. (c) O 2p orbitals located in between the Co^{3+} site and the Co^{4+} site. The blue (red) O 2p orbitals can hybridize with the Co^{3+} (Co^{4+}) site. (d) O 1s XAS spectra of Li_xCoO_2 ($x = 0.99, 0.66, 0.46,$ and 0.25) taken at incidence angle of 60° degrees.

site in between the Co^{3+} and Co^{4+} sites, the final states are the O 2p orbitals mixed into the Co^{3+} site or the Co^{4+} site due to the edge-sharing CoO_6 geometry [Fig. 1(c)]. In the present work, we have systematically investigated the electronic configuration and orbital anisotropy of Li_xCoO_2 single crystals with $x = 0.99, 0.66, 0.46,$ and 0.25 , using polarization dependent x-ray absorption spectroscopy (XAS) at the O 1s and Co 2p edges.

Single crystals of Li_xCoO_2 with $x = 0.99, 0.66, 0.46,$ and 0.25 were prepared as reported by Miyoshi *et al.* [17]. The XAS measurements were performed at 11ID-1 (spherical grating monochromator beam line) of the Canadian Light Source. The total-energy resolution was 100 meV. The base pressure of the XAS chamber was in

the 10^{-8} Pa range. The thin plate crystals were cleaved *in situ* in order to obtain clean surfaces which are parallel to the CoO_2 layers in Li_xCoO_2 . The spectra were measured in the total-electron-yield mode. All the spectra were measured at 20 K.

Figure 1(d) shows the O 1s XAS spectra of Li_xCoO_2 single crystals ($x = 0.99, 0.66, 0.46,$ and 0.25) for the incidence angle θ of 0° (normal incidence). While the O 1s XAS spectrum for $x = 0.99$ is dominated by the strong absorption peak at 530.5 eV, the spectra for $x = 0.66, 0.46,$ and 0.25 have three structures that are labeled as $\alpha, \beta,$ and γ . Whereas the γ structure loses its weight with decreasing x , α and β structures gain intensity. Therefore, the three structures labeled as $\alpha, \beta,$ and γ in the O 1s spectra can be assigned to the two absorption processes of the Co^{4+} state (α and β) and the one absorption process of the Co^{3+} state (γ) as shown in Fig. 1(b). The energy separation between structures β and γ indicates that the Co^{3+} and Co^{4+} species are almost frozen in the time scale of the O 1s to O 2p transition (order of femtosecond). Such separation can be understood on the basis of the polaron picture. Namely, the Co^{4+} state with $S = 1/2$ is trapped by the local lattice distortion in the background of the $S = 0$ Co^{3+} state. Surprisingly, the separation between Co^{3+} and Co^{4+} is still observed even in the highly oxidized samples of $x = 0.46$ and 0.25 with high electronic conductivity.

In order to examine the electronic structure with respect to the energy separation between the Co^{3+} and Co^{4+} species, we have performed model Hartree-Fock calculations for the CoO_2 triangular lattice [18]. The density of states and the band dispersions considering the CoO_2 layers were calculated by the unrestricted Hartree-Fock approach with the d - p Hamiltonian. Various parameters were determined by the cluster-model calculation of the Co 2p XPS spectra of the same samples. $\Delta, U,$ and $(pd\sigma)$ were found to be 1.0, 6.5, and -2.2 eV, respectively. Here, the ratio $(pd\sigma)/(pd\pi)$ is -2.16 . Remaining transfer integrals expressed by $(pp\sigma), (pp\pi), (dd\sigma),$ and $(dd\pi)$ are fixed at $-0.6, 0.15, -0.3,$ and 0.15 eV, respectively, for the undistorted lattice with the regular CoO_6 octahedron. When the lattice is distorted, the transfer integrals are scaled using Harrison's law. Here Δ denotes the charge-transfer energy for Co^{3+} or specifically $\Delta = \epsilon_d - \epsilon_p + 6U$.

The partial density of states (PDOS) of the Co 3d and O 2p orbitals were calculated for the various $\text{Co}^{3+}/\text{Co}^{4+}$ charge ordered states as shown in Fig. 2(a). In the unoccupied part of the calculated density of states the Co 3d PDOS and O 2p PDOS have three peaks. The highest energy peak loses its intensity with decreasing x or decreasing Co^{3+} concentration and can be assigned to the Co^{3+} component. On the other hand, the intensities of the lowest and middle peaks decrease with x , indicating that these two peaks are derived from the Co^{4+} component. The overall band structure change by the delithiation or by the reduction of x is consistent with the O 1s XAS results. As typical Co^{3+}

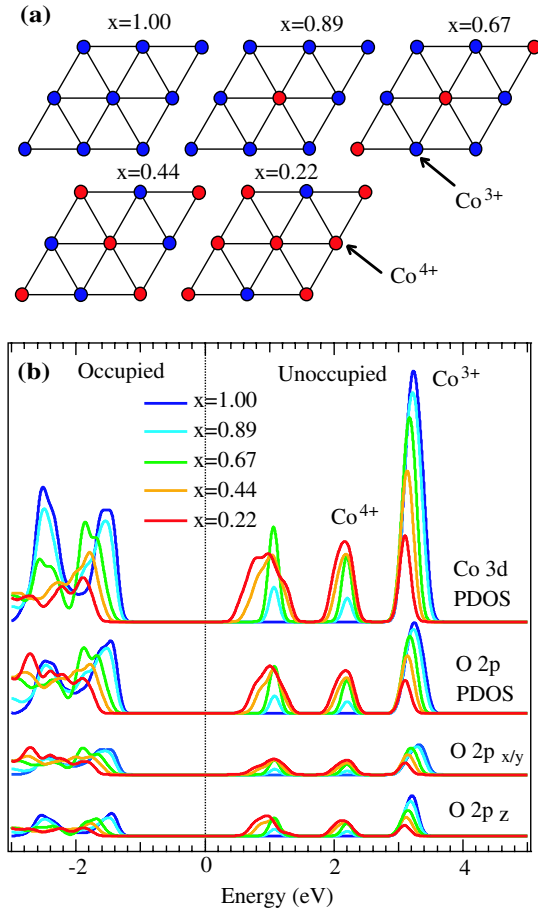


FIG. 2 (color online). (a) Schematic picture of the charge ordered states for $x = 1.00, 0.89, 0.66, 0.44,$ and 0.22 . The Co^{3+} and Co^{4+} sites are arranged with the ratio of $x:1-x$. (b) The $\text{Co } 3d$ and $\text{O } 2p$ PDOS calculated by the model Hartree-Fock methods for the charge ordered states.

oxides such as LaCoO_3 fall into the charge-transfer regime of the Zaanen-Sawatzky-Allen scheme, the unoccupied part for $x = 1.00$ (LiCoO_2) is dominated by the $\text{Co } 3d$ states while the $\text{Co } 3d$ and $\text{O } 2p$ components are heavily mixed in the occupied part. At $x = 0.89, 0.66, 0.44,$ and 0.22 , even the unoccupied states with the Co^{4+} origin have a substantial $\text{O } 2p$ character indicating that the Co^{4+} sites have more $\text{O } 2p$ holes than the Co^{3+} sites. This situation is schematically shown in Fig. 1(a) where the oxygen sites surrounding the Co^{4+} have more oxygen holes. Since the Li site is closer to the oxygen site than to the Co site, the Li-ion flow can be compensated by the oxygen hole back flow more effectively to minimize the lattice distortion due to the Li-ion motion.

The lowest and middle peaks in the $\text{O } 1s$ XAS spectra are assigned to the transitions to the $\text{O } 2p$ states mixed with the $\text{Co } 3d t_{2g}$ and e_g levels of the Co^{4+} sites. It is expected that the orbital anisotropy of the unoccupied $\text{Co } 3d t_{2g}$ and $\text{O } 2p$ states would be manifest in the incidence angle dependence of the XAS spectra. Figure 3 shows the $\text{O } 1s$ XAS spectra of Li_xCoO_2 ($x = 0.99, 0.66, 0.46$) for incident angles θ of 0° and 60° . Assuming that the $\text{Co } 3d e_g$ orbitals

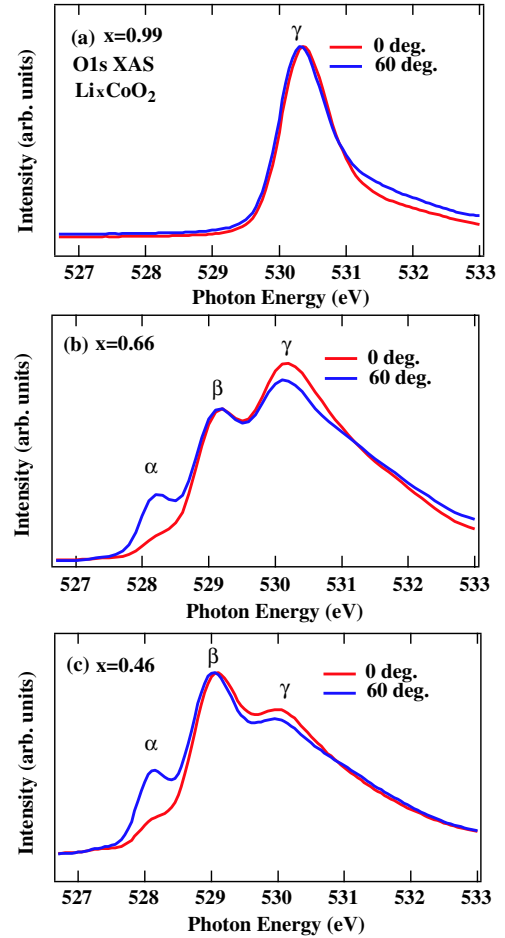


FIG. 3 (color online). $\text{O } 1s$ XAS spectra of Li_xCoO_2 at 20 K as a function of incidence angle for (a) $x = 0.99$, (b) $x = 0.66$, (c) $x = 0.46$.

of the Co^{4+} state are fully unoccupied and the total electron distribution is spherical, the $\text{O } 1s$ XAS spectra can be normalized using the intensity of structure β . Then the angle dependence of structure α reflects the polarization dependence of the transition strength from the $\text{O } 1s$ state to the anisotropic $\text{O } 2p$ states mixed with the anisotropic t_{2g} orbitals. The hole population in the a_{1g} and e'_g orbitals can be estimated from the angular dependence of structure α . In the $\text{O } 1s$ spectra of $\text{Bi}_2\text{Sr}_2\text{Co}_2\text{O}_9$ and Na_xCoO_2 with the CoO_2 triangular lattice, the intensity of structure α is strongly reduced at $\theta = 0^\circ$ and rapidly increases with θ , indicating that lowest energy holes are mainly located in the a_{1g} level [19,20]. The present results for Li_xCoO_2 also show that the unoccupied t_{2g} level is dominated by the a_{1g} component. Interestingly, the observed orbital anisotropy is consistent with the local density approximation band structure calculation which predicts that only the a_{1g} band crosses the Fermi level and the unoccupied part of the t_{2g} level is dominated by the a_{1g} component [21,22]. This agreement suggests that the lowest unoccupied states (constructed from the $\text{Co } 3d$ and $\text{O } 2p$ orbitals) with the a_{1g}

symmetry are highly itinerant and coexist with the more localized O $2p$ holes with e_g symmetry. This picture is consistent with the fact that the e_g states in O $1s$ XAS are split into the Co^{3+} and Co^{4+} components and the a_{1g} state in O $1s$ XAS is not. Here, it should be noted that we need to assume the $\text{Co}^{3+}/\text{Co}^{4+}$ charge order in the Hartree-Fock calculations with finite unit cell and, therefore, the band gap opens in the a_{1g} band. In Li_xCoO_2 , the Co^{3+} and Co^{4+} sites are at least partially disordered with the charge fluctuation. In this situation, the a_{1g} state can form the strongly renormalized metallic band as discussed in the theoretical work by Peil, Georges, and Lechermann [23].

Figure 4(a) shows the Co $2p$ XAS spectra of Li_xCoO_2 ($x = 0.99, 0.66, 0.46,$ and 0.25) for an incident angle θ of 60° . The Co $2p$ XAS spectra are normalized using the peak height of the main peak. The $2p_{3/2}$ and $2p_{1/2}$ peaks are

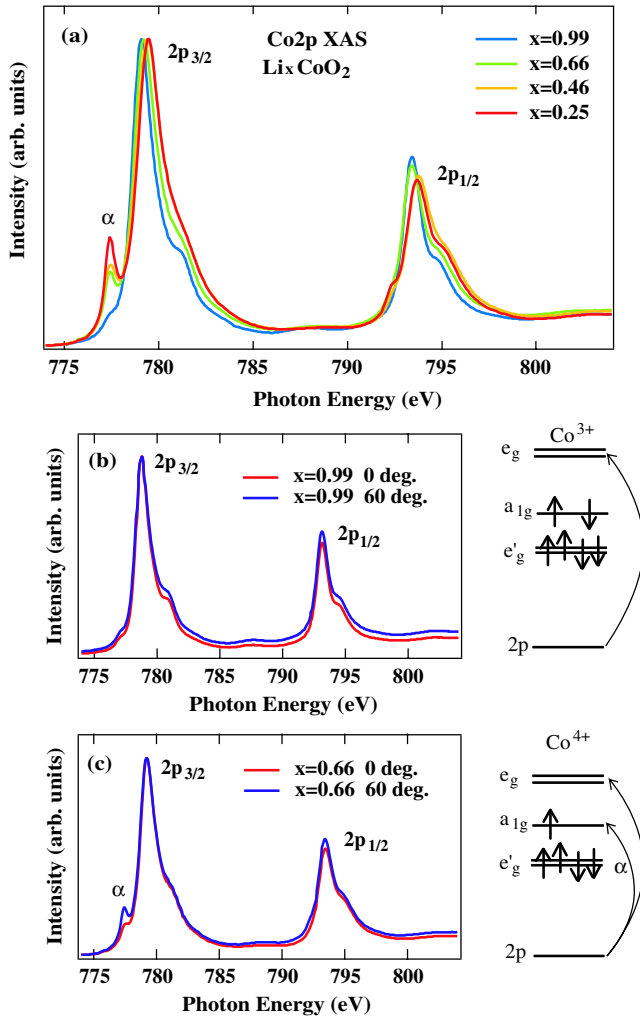


FIG. 4 (color online). (a) Co $2p$ XAS spectra of Li_xCoO_2 ($x = 0.99, 0.66, 0.46,$ and 0.25) at 20 K for the incidence angle θ of 60° . (b) Co $2p$ XAS spectra of Li_xCoO_2 ($x = 0.99$) at 20 K as a function of incidence angle. (c) Co $2p$ XAS spectra of Li_xCoO_2 ($x = 0.66$) at 20 K as a function of incidence angle.

very sharp with relatively small multiplet splitting, suggesting that the Co ions are in the low-spin state character [24] with fully unoccupied e_g states. This is supported by the fact that structures β and γ in the O $1s$ XAS show little angular dependence, which is only expected if the e_g states are fully unoccupied. Figures 4(b) and 4(c) show the Co $2p$ XAS spectra of Li_xCoO_2 ($x = 0.99$ and 0.66) for the incident angles θ of 0° and 60° . The intensity of structure α in the Co $2p$ XAS spectra increases in going from θ of 0° to 60° which is consistent with the angular dependence of structure α in the O $1s$ XAS spectra. It is observed that the intensity of structure α in the Co $2p$ XAS spectra also increases with decreasing x . This result indicates that the holes in Li_xCoO_2 are located in the a_{1g} band.

In Li_xCoO_2 with $x > 0.4$, the resistivity exhibits metallic behaviors whereas the magnetic susceptibility indicates localized spins [17,25,26]. Such dual behavior with itinerancy and localization of the Co $3d$ and O $2p$ states is consistent with the photoemission results on Li_xCoO_2 [26,27] in the wide range of x . Since the O $2p$ contribution in the Co^{4+} e_g state is much larger than that in the Co^{3+} e_g state, the e_g component of the O $2p$ holes tend to be localized as indicated by the present XAS results at 20 K. The photoemission results on the same system [27] show that the localized nature does not change appreciably up to 300 K. The present Hartree-Fock calculation for $\text{Co}^{3+}/\text{Co}^{4+}$ charge ordering can describe the overall features of the O $1s$ XAS spectra dominated by the localized part whereas it fails to describe the metallic a_{1g} state. The interplay between the localized e_g and itinerant a_{1g} components can provide the dual nature of Li_xCoO_2 . In the phase diagram of Li_xCoO_2 , since the lattice constant along the c axis increases with decreasing x [28,29], the CoO_6 octahedron becomes elongated along the c axis, and the ligand field effect shifts the a_{1g} level upwards. Although the upward shift of the a_{1g} level may increase its itinerancy, the unoccupied t_{2g} state is fully polarized to a_{1g} even in the large x region, and the increase of the c -axis lattice constant does not affect the angular dependence of the XAS spectra. In the future, in order to identify the electronic structure changes by the possible spin and/or charge orderings in Li_xCoO_2 , low energy excitations of the system should be studied using resonant inelastic x-ray scattering and angle-resolved photoemission spectroscopy.

In conclusion, we have studied the fundamental electronic structure of Li_xCoO_2 single crystals ($x = 0.99, 0.66, 0.46,$ and 0.25) which have CoO_2 triangular lattices with $\text{Co}^{3+}/\text{Co}^{4+}$ mixed valence. The Co $2p$ XAS spectra show that the Co^{3+} and Co^{4+} states are in the low-spin configurations even in the highly oxidized samples of $x = 0.46$ and 0.25 . The Co^{3+} and Co^{4+} species are separately observed in the O $1s$ XAS spectra. The comparison with the model Hartree-Fock calculation shows that the Co^{4+} state has more O $2p$ holes than the Co^{3+} state, and the difference in the O $2p$ hole amplitude is the origin of the

Co^{3+} - Co^{4+} separation. On the other hand, the lowest energy Co $3d$ t_{2g} level (which has a substantial O $2p$ component) has a_{1g} orbital symmetry and is highly itinerant. We propose that the localized e_g component of the O $2p$ holes can screen the Li-ion charge very effectively to enhance the Li-ion conductivity while the itinerant a_{1g} component contributes to the good electronic conductivity. The present study shows that the oxygen hole state in high valence transition-metal oxides is a key issue in the strategy to develop new cathode materials for wider applications.

We thank D. I. Khomskii, Z. Hu, L. H. Tjeng, K. Ikeda, M. Ohkubo, and I. Honma for fruitful discussions. This work is partially supported by Grants-in-Aid for Scientific Research from Japan Society for the Promotion of Science (JSPS), Funding Program for World-Leading Innovative R&D on Science and Technology (FIRST Program), and Toray Science Foundation. The Canadian based research was funded in part by NSERC, CIFAR, CFI, and CRC. The XAS experiments were carried out at beam line 11ID-1, Canadian Light Source (proposal ID: 11-2170).

-
- [1] K. Mizushima, P. C. Jones, P. J. Wiseman, and J. B. Goodenough, *Mater. Res. Bull.* **15**, 783 (1980).
- [2] J. Zaanen, G. A. Sawatzky, and J. W. Allen, *Phys. Rev. Lett.* **55**, 418 (1985).
- [3] A. E. Bocquet, T. Mizokawa, T. Saitoh, H. Namatame, and A. Fujimori, *Phys. Rev. B* **46**, 3771 (1992).
- [4] M. K. Aydinol, A. F. Kohan, G. Ceder, K. Cho, and J. Joannopoulos, *Phys. Rev. B* **56**, 1354 (1997).
- [5] A. K. Padhi, K. S. Nanjundaswamy, and J. B. Goodenough, *J. Electrochem. Soc.* **144**, 1188 (1997).
- [6] K. Takada, H. Sakurai, E. Takayama-Muromachi, F. Izumi, R. A. Dilanian, and T. Sasaki, *Nature (London)* **422**, 53 (2003).
- [7] I. Terasaki, Y. Sasago, and K. Uchinokura, *Phys. Rev. B* **56**, R12685 (1997).
- [8] M. L. Foo, Y. Wang, S. Watauchi, H. W. Zandbergen, T. He, R. J. Cava, and N. P. Ong, *Phys. Rev. Lett.* **92**, 247001 (2004).
- [9] E. Plichta, S. Slane, M. Uchiyama, M. Salomon, D. Chua, W. B. Ebner, and H. W. Lin, *J. Electrochem. Soc.* **136**, 1865 (1989).
- [10] H. F. Gibbard, *J. Power Sources* **26**, 81 (1989).
- [11] T. Nagaura and K. Tazawa, *Prog. Batteries Sol. Cells* **9**, 20 (1990).
- [12] A. Honders, J. M. der Kinderen, A. H. van Heeren, J. H. de Wit, and G. H. J. Broers, *Solid State Ionics* **14**, 205 (1984).
- [13] J. Molenda, C. Delmas, P. Dordor, and A. Stoklosa, *Solid State Ionics* **12**, 473 (1984).
- [14] M. Ménétrier, I. Saadouné, S. Lévassieur, and C. Delmas, *J. Mater. Chem.* **9**, 1135 (1999).
- [15] J. van Elp, J. L. Wieland, H. Eskes, P. Kuiper, G. A. Sawatzky, F. M. F. de Groot, and T. S. Turner, *Phys. Rev. B* **44**, 6090 (1991).
- [16] M. T. Czyżyk, R. Potze, and G. A. Sawatzky, *Phys. Rev. B* **46**, 3729 (1992).
- [17] K. Miyoshi, C. Iwai, H. Kondo, M. Miura, S. Nishigori, and J. Takeuchi, *Phys. Rev. B* **82**, 075113 (2010).
- [18] T. Mizokawa and A. Fujimori, *Phys. Rev. B* **54**, 5368 (1996).
- [19] T. Mizokawa, L. H. Tjeng, P. G. Steeneken, N. B. Brookes, I. Tsukada, T. Yamamoto, and K. Uchinokura, *Phys. Rev. B* **64**, 115104 (2001).
- [20] W. B. Wu, D. J. Huang, J. Okamoto, A. Tanaka, H.-J. Lin, F. C. Chou, A. Fujimori, and C. T. Chen, *Phys. Rev. Lett.* **94**, 146402 (2005).
- [21] D. J. Singh, *Phys. Rev. B* **61**, 13397 (2000).
- [22] C. A. Marianetti, G. Kotliar, and G. Ceder, *Nat. Mater.* **3**, 627 (2004).
- [23] O. E. Peil, A. Georges, and F. Lechermann, *Phys. Rev. Lett.* **107**, 236404 (2011).
- [24] H.-J. Lin, Y. Y. Chin, Z. Hu, G. J. Shu, F. C. Chou, H. Ohta, K. Yoshimura, S. Hébert, A. Maignan, A. Tanaka, L. H. Tjeng, and C. T. Chen, *Phys. Rev. B* **81**, 115138 (2010).
- [25] T. Motohashi, T. Ono, Y. Sugimoto, Y. Masubuchi, S. Kikkawa, R. Kanno, M. Karppinen, and H. Yamauchi, *Phys. Rev. B* **80**, 165114 (2009).
- [26] S. Laubach, S. Laubach, P. C. Schmidt, D. Enslin, S. Schmid, W. Jaegermann, A. Thisen, K. Nikolowski, and H. Ehrenberge, *Phys. Chem. Chem. Phys.* **11**, 3278 (2009).
- [27] K. Ikeda, Y. Wakisaka, T. Mizokawa, C. Iwai, K. Miyoshi, and J. Takeuchi, *Phys. Rev. B* **82**, 075126 (2010).
- [28] A. Van der Ven, M. K. Aydinol, G. Ceder, G. Kresse, and J. Hafner, *Phys. Rev. B* **58**, 2975 (1998).
- [29] G. G. Amatucci, J. M. Tarascon, and L. C. Klein, *J. Electrochem. Soc.* **143**, 1114 (1996).